ARTICLE

Continuous medium exchange and optically induced electroporation of cells in an integrated microfluidic system

Gwo-Bin Lee[1,2,3], Chia-Jung Chang[1], Chih-Hung Wang[1], Ming-Yu Lu[1] and Yen-Yi Luo[1]

Optically induced electroporation (OIE) is a promising microfluidic-based approach for the electroporation of cell membranes. However, previously proposed microfluidic cell-electroporation devices required tedious sample pre-treatment steps, specifically, periodic media exchange. To enable the use of this OIE process in a practical protocol, we developed a new design for a microfluidic device that can perform continuous OIE; i.e., it is capable of automatically replacing the culture medium with electroporation buffers. Integrating medium exchanges on-chip with OIE minimises critical issues such as cell loss and damage, both of which are common in traditional, centrifuge-based approaches. Most importantly, our new system is suitable for handling small or rare cell populations. Two medium exchange modules, including a micropost array railing structure and a deterministic lateral displacement structure, were first adopted and optimised for medium exchange and then integrated with the OIE module. The efficacy of these integrated microfluidic systems was demonstrated by transfecting an enhanced green fluorescent protein (EGFP) plasmid into human embryonic kidney 293T cells, with an efficiency of 8.3%. This result is the highest efficiency reported for any existing OIE-based microfluidic system. In addition, successful co-transfections of three distinct plasmids (EGFP, DsRed and ECFP) into cells were successfully achieved. Hence, we demonstrated that this system is capable of automatically performing multiple gene transfections into mammalian cells.

Keywords: electroporation; medium exchange; microfluidic; transfection

Microsystems & Nanoengineering (2015) 1, 15007; doi:10.1038/micronano.2015.7; Published online: 15 June 2015

INTRODUCTION

In the past few decades, single-function microfluidic components capable of performing specific tasks, such as cell separation[1–4], particle/cell focusing[5] and cell electroporation[6–8], have been thoroughly investigated as stand-alone components in a variety of microfluidic applications. However, in terms of replacing a traditional clinical laboratory with a single lab-on-a-chip, most of these stand-alone microfluidic components were not sufficient to address practical problems that require multiple processing steps. For example, in electroporation, mammalian cells must be transferred from the original culture medium into a specialised electroporation buffer to optimise the electroporation yield[9–11]. Existing microfluidic electroporation devices are incapable of performing this sample pre-treatment step, and the inherent advantages of microfluidic lab-on-a-chip systems, such as automation, user friendliness and the reduction of human error, were compromised. Therefore, a real need exists to develop a microscale total analysis system integrated with different functional microfluidic components to truly leverage the advantages of the aforementioned microfluidic systems.

The cell membrane acts as a barrier to prevent intracellular molecules from randomly being delivered into the interior of cells. Conventional cell electroporation disrupts the integrity of the cell membrane using a short electrical pulse. Electroporation increases the permeability of the cell membrane to allow chemicals, drugs or foreign DNA chains, to enter into cells for biological and medical applications. For successful cell electroporation, the target adherent cells also must be trypsinised, washed, and then transferred into a specialised electroporation buffer to optimise electroporation yield. Furthermore, because of the relatively large size of the electroporation apparatus, a high voltage is commonly used to generate the required electric field for electroporation. This high voltage and the relatively complicated protocol can easily damage the target cells; this protocol also presents a risk of injury to the operator. Hence, the cell viability rate after traditional electroporation is typically less than 50% for mammalian cell lines[12].

Recently, electroporation was integrated into microfluidic devices by using various types of mechanisms[13–17]. In comparison to conventional electroporation methods, microfluidic systems have some advantages, including the use of a lower applied electric field, lower sample and reagent consumption and reduced Joule heating[6]. However, existing microfluidic electroporation devices with fixed micro-electrodes are incapable of exchanging media in a sample pre-treatment step. In addition, the fabrication of delicate microelectrodes may also hinder their practical application.

Optically induced electroporation (OIE), also known as light-induced electroporation, is a microfluidic approach for cell electroporation that offers significant flexibility with respect to other methods requiring fixed metal electrodes[15]. The OIE system enables the operator to quickly reconfigure the electrode geometries and locations to perform different electroporation applications without having to re-fabricate the entire chip[18]. Multiple single cells can be optically targeted for electroporation in parallel by dynamically adjusting the "virtual electrodes" projected by the digitally controlled light patterns. This precision control of the electrode leaves the other cells unaffected. External substances, such

[1]Department of Power Mechanical Engineering, National Tsing Hua University, Hsinchu 30013; [2]Institute of Biomedical Engineering, National Tsing Hua University, Hsinchu 30013 and [3]Institute of NanoEngineering and Microsystems, National Tsing Hua University, Hsinchu 30013
Correspondence: Gwo-Bin Lee (gwobin@pme.nthu.edu.tw)

as fluorescent dyes and genes, have been successfully transferred into mammalian cells using this method[15,19]. However, a proper electroporation buffer (such as a 0.2 M sucrose solution) is commonly used to generate sufficient transmembrane potentials on cells for OIE[19]. Therefore, the re-suspended cells must be centrifuged in advance to replace the original culture medium with the proper electroporation buffer. Thus, this centrifuging step makes cell electroporation a complicated process.

Microfluidic-based devices for cell separation can be divided into two categories: active or passive approaches. Active microfluidic devices require an external force to control fluid transfer and for cell separation. For example, we previously reported a microfiltering structure to collect cells for the subsequent optically induced cell separation process[20]. Up to 96.2% of the live cells loaded into the microfluidic device were successfully recovered. However, this device required a precision micropump for flow control. Alternatively, several passive microfluidic approaches to sort and to manipulate cells have been demonstrated previously. For example, a deterministic lateral displacement (DLD) structure is a promising microfluidic technique to separate particles and cells based on their sizes, shape and deformability[21–23]. DLD is a passive, hydrodynamics-based particle-sorting technique that consists of a symmetric array of micro-posts[22,24]. The hydrodynamic interaction between particles and the microstructures enables the separation of particles with different sizes. A larger particle is deflected at a specific angle and then transferred to another flow stream. By contrast, a smaller particle is not affected by these interactions and hence is not laterally displaced. In addition, DLD is able to steer, refract and focus streams of biomaterials and has been implemented in various biomedical applications[23,25–30]. A micro-post array railing (µPAR) structure is another passive, hydrodynamics-based particle-sorting technique[31]. The µPAR structure consists of an array of square micro-posts that are tilted at a specific angle with respect to the fluid flow direction. The gaps between micro-posts are smaller than the suspended target particles or cells and could therefore guide them into discrete, adjacent laminar flow streams. This structure had been demonstrated to automatically perform molecular synthesis processes on polystyrene microbead substrates while simultaneously mixing suspended cells with discrete, parallel flow streams[31,32]. Note that the DLD or µPAR microstructures were originally demonstrated for the separation of particles or cells. In this work, DLD or µPAR microstructures have been adopted to guide cells into a certain direction so that medium exchange could be performed continuously.

Herein, a novel microfluidic device was developed that combines both OIE and medium exchange functions into an integrated system. The continuous medium exchange and electroporation of the cells is performed by the medium exchange modules consisting of µPAR or DLD structures and the OIE module, respectively. This system enables a completely integrated cell electroporation workflow. Finally, single or co-transfection of three types of fluorescently labelled plasmids into HEK 293T cells was successfully demonstrated using this OIE microfluidic system. These results show that this microfluidic system is a promising tool for genetic engineering.

MATERIALS AND METHODS

Design of the integrated microfluidic system

The developed integrated microfluidic system has two modules connected in series: the medium exchange and the OIE modules, as schematically shown in Figure 1. First, the re-suspended cells in the original culture medium were transferred into the electroporation buffer by using one of the passive medium exchange modules. Next, the electroporation buffer carrying the cells flows into the OIE module, where electroporation occurs.
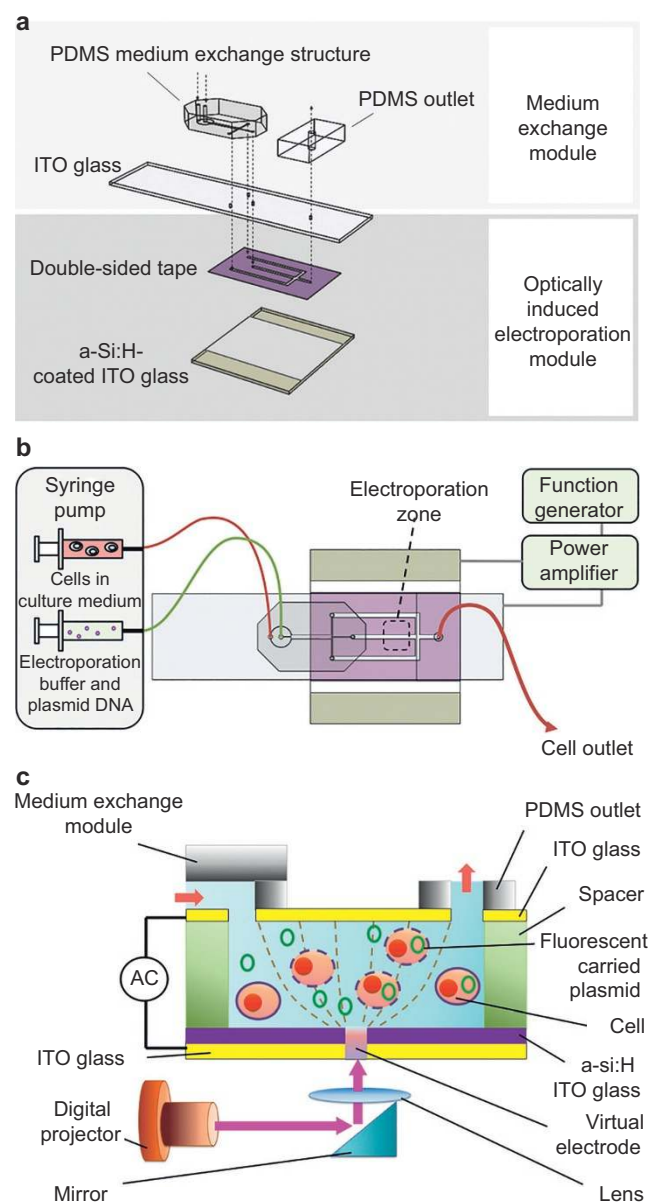

Figure 1 (a) The integrated microfluidic device was composed of two modules: a continuous medium exchange module and an OIE module. The continuous medium exchange module consisted of a patterned PDMS structure bonded to a layer of glass substrate. The OIE module was formed by bonding a top layer of ITO glass to a bottom layer of a-Si:H coated ITO glass with double-sided tape that is patterned by a CO_2 laser. The fluid channels in both modules were 50 µm in height. The modules were connected by through holes drilled at the interface between the two modules. The processed fluid was collected from the single PDMS outlet located at the rear of the integrated device. (b) Syringe pumps were used to inject the cells suspended in the culture medium and the electroporation buffer to flow through the medium exchange module. Next, the cells were transferred into the electroporation buffer stream (which contained the plasmid DNA), electroporated in the OIE zone in the OIE module and then collected at the outlet. (c) The working principle of OIE-based microfluidic chip. The target cell and fluorescently labelled plasmid were transported into the OIE module. A digital projector illuminated a light spot onto the bottom of a-Si:H layer, which generated a virtual electrode. Next, the fluorescently labelled plasmids were electroporated into the target cell. Finally, the electroporated cells were collected at the outlet and cultured for further analysis.

As schematically shown in Figure 1a, the continuously flowing, passive medium exchange module consisted of a patterned polydimethylsiloxane (PDMS) structure bonded to a layer of indium-tin-oxide (ITO) glass substrate. The OIE module was formed by bonding the top layer of ITO glass to a bottom layer of hydrogen-rich amorphous-silicon (a-Si:H)-coated ITO glass with double-sided tape patterned by a CO_2 laser. The modules were connected via through holes drilled at the interface between the two modules while the processed fluid was collected from the single PDMS outlet located at the top of the integrated device.

Experimental setup

An illustration of the OIE chip is shown in Figure 1b. The developed chip was mounted on an upright fluorescence microscope (BX43, Olympus Co., Japan) that allowed for real-time observation using a charge-coupled device (CCD) camera (Evolution VF, Media Cybernetics, Inc., USA). Two fluid streams of (1) medium with cells and (2) electroporation buffer with fluorescently labelled plasmids were continuously injected into the microfluidic chip using two syringe pumps (KDS-270, KD Scientific, USA). Note that double-side tape was used as a spacer. Cells, reagents and buffers were first introduced from the through-hole of the PDMS inlet, and then the entire process, i.e., medium exchange and OIE was performed automatically. The position of the virtual electrodes was determined by the projected light pattern, which was generated by the digital projector. The re-suspended cells were transferred from the culture media into the flowing electroporation buffer using DLD or μPAR structures. Figure 1c shows a cross-sectional view of the device that describes the working principle of the optically induced gene transfection. The target cell and fluorescently labelled plasmid were transported via the electroporation buffer into the lower OIE module. A digital projector (PLC-XU106, SANYO Electric Co., Japan) illuminated a light spot onto the a-Si:H layer, which acted as a virtual electrode in the electroporation zone. The alternating-current (AC) voltage was generated by a function generator (AFG-2125, Good Will Instrument Co., Ltd., Taibei) and amplified by a power amplifier (HA-405, PINTEK, New Taipei City). This established an AC electric field between the top and bottom ITO layers. Next, the fluorescently labelled plasmids were electroporated into the target cell. The output voltage was monitored using an oscilloscope (GDS-1102-U, Good Will Instrument Co., Kaohsiung). Finally, the electroporated cells were collected at the outlet and cultured for further analysis.

Design of medium exchange modules: DLD and μPAR

To transfer the cells from the original culture medium into the electroporation buffer, the culture medium with suspended cells was injected into the outer flow. The target cell was guided to the central stream of the electroporation buffer by the DLD structures (Figure 2a). The DLD design parameters, $\lambda = 60$ μm, $\varepsilon = 0.05$, gap = 30 μm, correspond to a critical particle diameter (Dc) of ~9 μm and the scanning electron microscope (SEM) image of the DLD microstructure is presented in Figure 2b. Therefore, any target HEK 293T cells greater than 9 μm in diameter fell into the "bump mode" category and could be theoretically transferred into the buffer stream[22].

For the μPAR structure, the re-suspended cells in the outer streams were guided into the centre of the electroporation buffer stream by the μPAR structure (Figure 2c). Next, the cells were electroporated using OIE. The μPAR structure consisted of tilted arrays of rectangular micro-posts with gaps smaller than the diameter of the cells. The length of the sides of the micro-posts was 20 μm, and the gap between micro-posts was 10 μm. The tilt

angle of the arrays with respect to the fluid flow, α, was 1°, and the SEM image of the μPAR microstructure is presented in Figure 2d.

Fabrication of the medium exchange modules

The medium exchange modules were micro-fabricated by bonding PDMS fluid channels onto the non-conducting side of the ITO glass substrate. A 50 μm thick layer of negative photoresist SU-8 3050 (MicroChem Corp., USA) was photolithographically patterned as a mould and was used to replicate the inverse structure in PDMS. First, a bare silicon wafer substrate was rinsed with double-distilled water (ddH$_2$O) and then sonicated for 5 min in acetone to detach any particles from the surface. Next, the treated wafer was rinsed with ddH$_2$O and then air dried. Afterwards, the wafer was treated with a buffered-oxide-etch (BOE) reagent, rinsed with ddH$_2$O and then dried again. Following the BOE treatment, the wafer was placed on a hotplate at 150 °C for 5 min to dehydrate the surface. After this substrate pre-treatment, the wafer was cooled down to room temperature, and then a layer of SU-8 50 with a thickness of 50 μm was spin-coated onto the surface using a spin-coater (200F, Filmtronics, USA). Next, the SU-8 was soft-baked at 65 °C for 6 min and then at 95 °C for 20 min to evaporate the solvent prior to exposure. Next, the wafer was cooled down to room temperature prior to exposure. The ultraviolet light exposure dosage for SU-8 was 250 mJ cm^{-2}. A two-step post exposure bake was performed immediately after the exposure at 65 °C for 1 min and then at 95 °C for 5 min. Finally, the developed pattern was rinsed with isopropyl alcohol and dried. As a final step, the wafer and SU-8 mould were placed on a hot plate at 175 °C for 4 hours to enhance the strength of the structure. This structure served as a negative mould for the PDMS. For casting the PDMS, an elastomer (Sylgard 184A silicon elastomer, Dow Corning, USA) and a curing agent (Sylgard 184B elastomer curing agent, Dow Corning, USA) were well mixed in a 10:1 ratio by weight, poured onto the SU-8 mould and then cured at 80 °C over 2 h to form the DLD and μPAR microstructures for medium exchange.

Fabrication of the OIE module and the integration of the two modules

The OIE channel was patterned on a piece of double-sided tape (50 μm in height; Tesa Tape, Inc., USA) by using a laser-cutting machine (VersaLASER VL-200, Universal Laser Systems, Inc., USA). The patterned tape was attached to the a-Si:H coated ITO glass, and then through-holes were drilled to form an OIE module. Finally, the drilled holes in the PDMS medium exchange structure and the PDMS outlet were aligned and bonded onto the top surface of the ITO glass via oxygen plasma treatment.

Preparation of human embryonic kidney 293T (HEK 293T) cells and electroporation buffer

Human embryonic kidney cells (HEK 293T, ATCC® CRL-11268TM) were provided by the Institute of Microbiology and Immunology, College of Medicine, Chung Shan Medical University, Taichung and cultured in Dulbecco's Modified Eagle Medium (DMEM), which contained 10% fetal bovine serum (Sigma Co., USA), 2 mM of L-glutamine (Sigma Co., USA) and 1% penicillin/streptomycin. The monolayer of cells was trypsinised with 1x trypsin-EDTA (Sigma Co., USA) and then re-suspended in DMEM, yielding a final concentration of 106 cells ml^{-1}. The pEGFP-N1 (4.7 kp), pDsRED (4.1 kp) and pECFP (4.1 kp) plasmids were provided by the Institute of Biomedical Sciences, National Sun Yat-Sen University, Kaohsiung. Note that the three fluorescently labelled plasmid DNAs were extracted with NucleoBond® Xtra Midi kits (MACHEREY
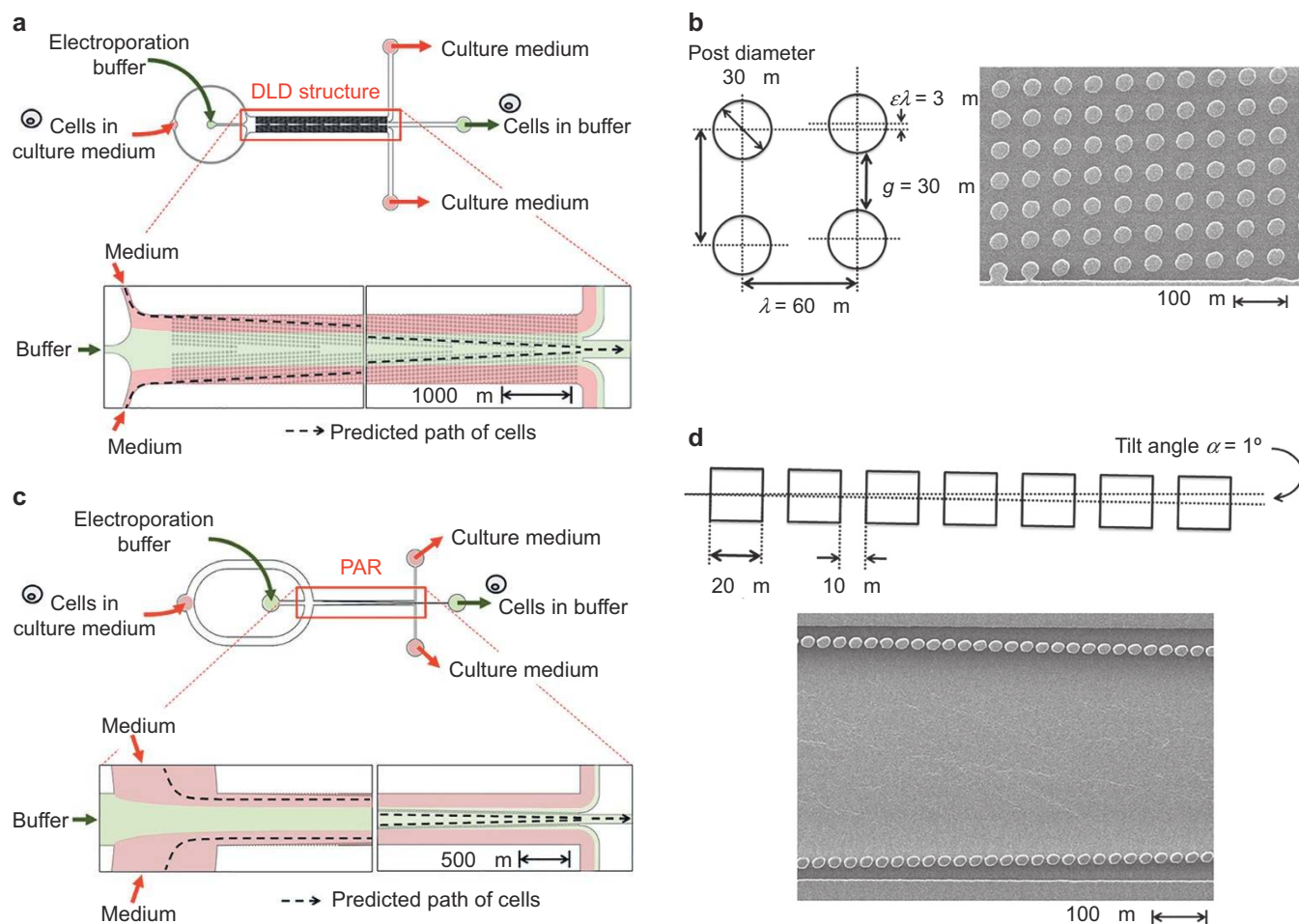
Figure 2 **(a)** Cells suspended in the culture medium were introduced into the medium exchange module consisting of a DLD structure and then were "bumped" into the central stream of the electroporation buffer. The dashed black lines represent the predicted path of the cells in the DLD structure. **(b)** The proposed DLD design parameters and a SEM image of the PDMS mould replica. Each post diameter is 30 μm, λ is 60 μm, ε is 0.05, and the gap between posts is 30 μm. The estimated critical particle diameter is approximately 9 μm. **(c)** Cells in the culture medium were introduced into the μPAR structure and then were guided into the central stream of the electroporation buffer. The dashed black lines are the predicted paths of cells in the μPAR structure. **(d)** Proposed μPAR design parameters and an SEM image of the PDMS mould replica. The length of the long side of each rectangular microposts is 20 μm, the gap between microposts is 10 μm, and the tilt angle is 1°.

NAGEL GmbH & Co, Germany), following the protocols in the user's manual. These extracted plasmid DNAs were re-suspended in 0.2 M sucrose (Sigma Co., USA) at a final concentration of 2 μg ml^{-1}.

OIE parameters

The optimised experimental parameters for the continuous medium exchange and the OIE experiment are presented in Table 1, which were based on the OIE simulations and the

Table 1 The operating conditions for continuous medium exchange and for the OIE experiments

Controlled parameters	Value (unit)
Applied AC frequency	20 (kHz)
Light irradiance	1.5 (W cm^{-2})
Size of "virtual electrode"	3.5 mm × 3.0 mm

practical operating limits of the instrumentation. Specifically, the applied AC frequency was designated to be just below the value that would cause hydrolysis in the OIE channel, and the light irradiance and light spot size were both set at stable conditions near the upper limits of the optical system.

RESULTS

Exchange efficiency of the medium exchange modules

Tests on the medium exchange modules were first performed to ensure the successful performance of the proposed device. The deflection of the cellular trajectory was observed in the DLD continuous medium exchange module (Figure 3a). The HEK 293T cells in the DLD structure were in the "bumping mode", where the trajectory of the cells was inclined at a specific tilt angle towards the centre of the channel, resulting in an overall lateral displacement that shifted the cells from the outer flow to the centre flow of the electroporation buffer. Note that the medium and buffer flows were injected using syringe pumps at the same flow rates of 25 μl min^{-1}. For the medium exchange module with

a

Flow direction

250 m

• HEK 293T cell

b

Flow direction   250 m

• HEK 293T cell
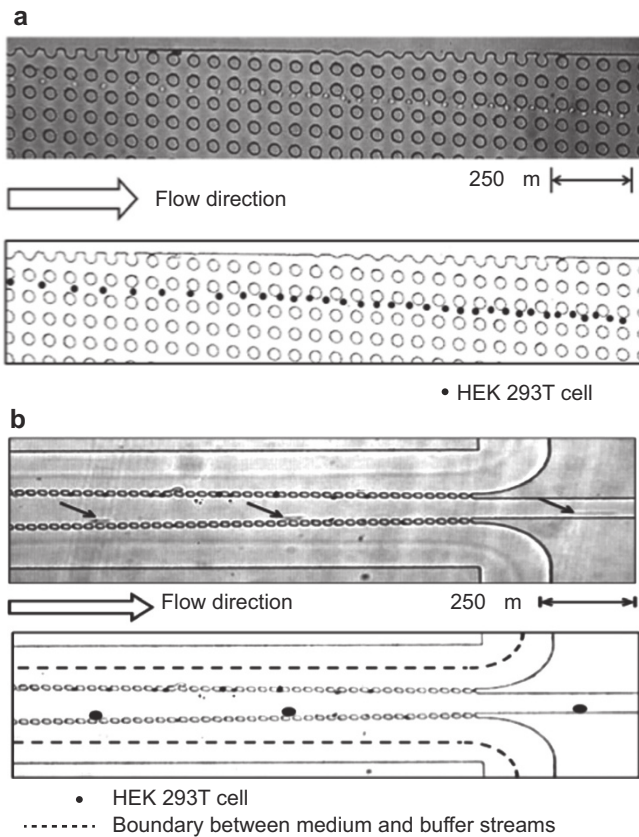- - - - - - - Boundary between medium and buffer streams

Figure 3 A composite time-lapsed image **(a)** of the continuous medium exchange with an HEK 293T cell in the DLD structure. The relative positions of the cell with respect to the DLD structure are represented by black dots. The cell was in "bumping mode" and was being deflected from the direction of liquid flow and transferred into the central stream of the electroporation buffer by the DLD structure. The time interval between images was 10 ms. **(b)** A composite time-lapsed image of the continuous medium exchange with an HEK 293T cell in the µPAR structure. The cells were guided into the central stream of the electroporation buffer by the µPAR structure. The relative positions of the cell and the flow boundaries of the inner culture medium and outer buffer streams with respect to the µPAR structure are represented by black dots. The time interval between images was 10 ms.

µPAR structures, the deflection in flow trajectory was also observed. The cells were guided toward the centre stream of the electroporation buffer by the micro-post arrays (Figure 3b). The continuous flows of cell culture medium and electroporation buffer streams were injected using syringe pumps set at the same flow rates of 70 µl min^{-1}.

To evaluate the performance of the two medium exchange modules, HEK 293T cells suspended in the culture medium and the electroporation buffer (0.2 M sucrose) were injected into the modules. The cells were collected from the three outlets of each module (one central outlet and two side outlets). For the DLD medium exchange module, the fluids were injected by the syringe pumps at the same corresponding volumetric flow rates, ranging from 30 to 90 µl min^{-1}. Alternatively, the fluids in the µPAR medium exchange module were driven by using a vacuum pump at the outlets with equally applied gauge pressures, ranging from −100 to −300 mmHg. The exchange efficiency was calculated by dividing the number of cells collected from the

central outlet by the number of total cells collected from all three outlets (as shown in Equation (1)).

$$\text{Exchange efficiency} = \frac{\text{Cells collected from the central outlet}}{\text{Total number of collected cells}} \times 100\%$$

(1)

The experimental results showed that the exchange efficiency was higher for the proposed µPAR module than the DLD module at different fluid flow rates. For the DLD medium exchange module, the exchange efficiency increased with increasing flow rate and saturated at high flow rates (Figure 4a). The highest exchange efficiency of 33.7% was observed at a volume flow rate of 90 µl min^{-1} (Figure 4a). In the µPAR medium exchange module, the exchange efficiency also increased with increasing flow rates. The stronger the vacuum suction, the faster the fluid flow and the higher the exchange efficiency. Saturation was also
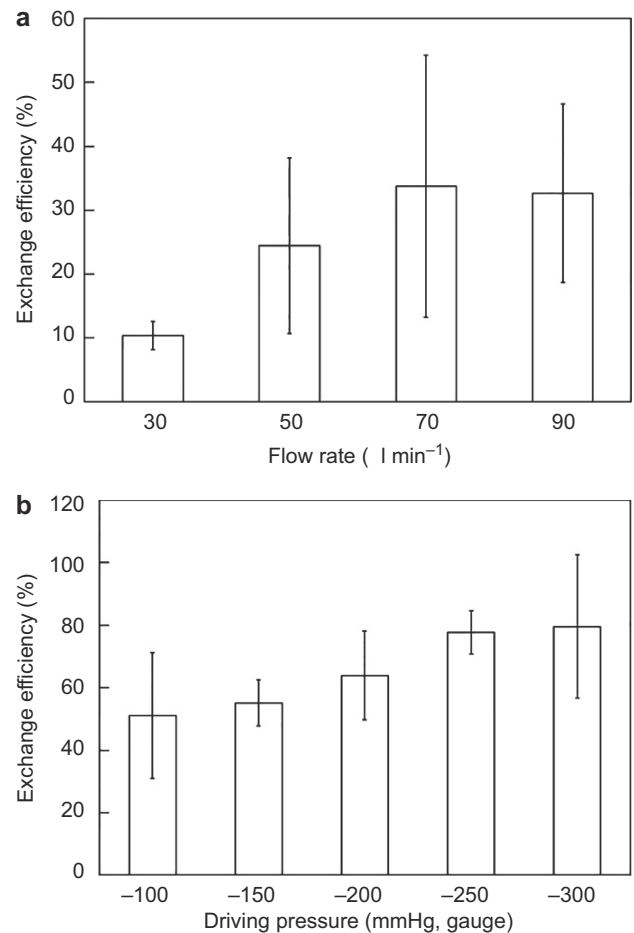
a

b

Figure 4 Exchange efficiency of HEK 293T cells processed by the **(a)** DLD microstructure and the **(b)** µPAR microstructure. **(a)** The data shows that the exchange efficiency is determined by different input flow rates of the syringe pump. This data suggests that the volume flow rate should be set higher than 90 µl min^{-1} to achieve the optimal exchange efficiency. **(b)** The exchange efficiency of the µPAR structure was measured with respect to the negative gauge pressure at the outlet. The device successfully exchanged 79.5% of the input cells into the electroporation buffer at an applied gauge pressure of −300 mmHg.

observed at higher flow rates (Figure 4b). The maximum value of the exchange efficiency for the µPAR medium exchange module was measured to be 79.5% at a gauge pressure of −300 mmHg (Figure 4b). Note that three consecutive experiments were performed for each test. Conventionally, µPAR and DLD microstructures were only used to separate mixed particles or cells in single buffer, depending on the size of particles[1,31]. However, µPAR and DLD were used to perform the medium exchange in this study, which represents the first time that these similar microstructures were used for medium exchange.

The effect of the size and the photoconductivity of the virtual electrode on the transmembrane potential

The effects of three independent parameters on the cell transmembrane potential, including the spot diameter of the illuminated pattern, the applied AC frequency and the photoconductivity of the a-Si:H film, were considered when inducing electroporation. Commercially available software (COMSOL Multiphysics, USA) was used to numerically simulate the cell transmembrane potential induced by the virtual electrode. To better understand the relationship between these parameters and the maximum transmembrane potential, the following parameters were used: the relative spot diameter, defined as the full width at half maximum divided by the cell diameter (12 µm), and the relative photoconductivity, defined as the a-Si:H photoconductivity divided by the conductivity of the medium outside the cell. The results of the numerical simulation showed that the maximum induced transmembrane potential generally increased with the increasing relative spot diameter and the relative photoconductivity. The dependence of the transmembrane potential on the relative spot diameter can be determined from the pattern of the voltage distribution under different spot diameters (Figure 5a), where the relative photoconductivity and the applied AC frequency were 0.1 and 1 kHz, respectively. For smaller spot diameters, the cell at the centre of the channel was less affected by the gradient of the voltage distribution across the electroporation buffer. As the diameter of the "virtual electrode" increased, the area of the voltage gradient expanded and reached the cell, inducing a larger transmembrane potential across the cell membrane. To determine the maximum transmembrane potential with respect to the driving frequency, the spot size and the photoconductivity, a simultaneous parametric sweep of all three variables was performed. The size of the black spheres represented the value of the maximum transmembrane potential under each condition (Figure 5b). In general, the induced transmembrane potential at a certain applied peak-to-peak voltage could be maximised by increasing the relative photoconductivity and the relative spot diameter, and decreasing the applied AC frequency.

Transfection of plasmid DNA using the integrated microfluidic system

In our previous work[33], fluorescence dyes (propidium iodide, PI and calcein acetoxymethyl ester, CaAM) were used to measure the electroporation efficiency when µPAR microstructures were used to perform the medium exchange. However, using fluorescent dyes to determine the electroporation efficiency is considered to be indirect evidence. In conventional electroporation or transfection experiments, plasmid DNA is commonly used to demonstrate the extent of gene transfection while developing novel methods or new systems[34]. Therefore, the fluorescence-carrying plasmid DNA was used to determine the efficiency of electroporation in this study.

Transfection of a pEGFP-N1 plasmid DNA was conducted to demonstrate the successful integration of the two modules. The use of HEK 293T cells, human embryonic kidney cells, has been
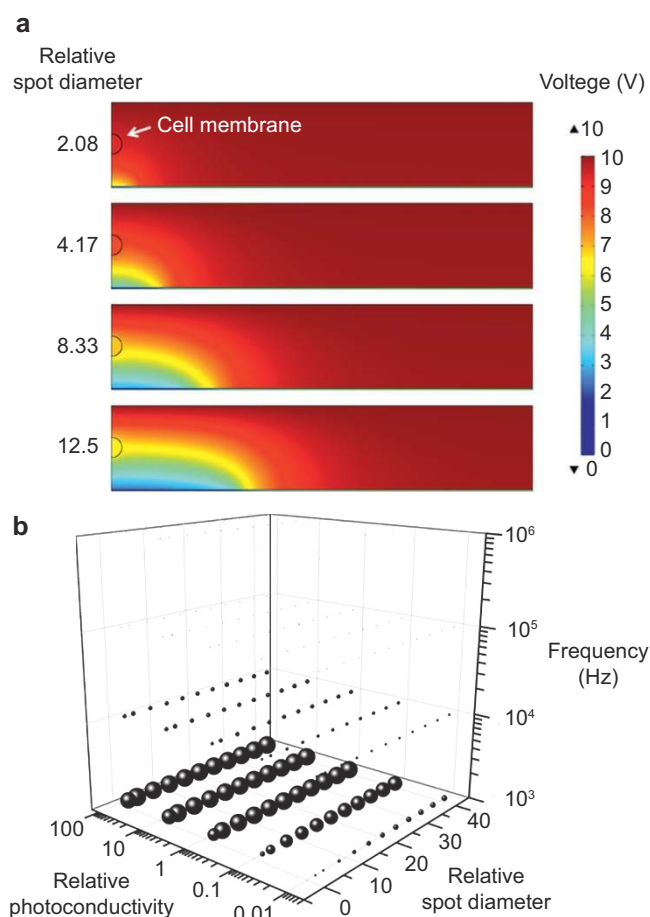

Figure 5 **(a)** The voltage distribution for different relative spot diameters under a relative photoconductivity of 0.1 and an applied AC frequency of 1 kHz. The results indicate that the cell is less affected under smaller relative spot diameters. **(b)** The OIE simulation results indicate that the transmembrane potential of the cell in the OIE device increased with increasing photoconductivity, larger electrode sizes, and decreasing frequency. The size of the black ball is proportional to the magnitude of the maximum transmembrane potential induced across the cell.

commonly reported for gene transfection and was used as a guideline template for many transfection kits (e.g. lipofectamine, Thermo Fisher Scientific Inc.)[32]. HEK 293T cells were re-suspended in a culture medium and the electroporation buffer (0.2 M sucrose) containing the plasmid DNA was injected into the complete integrated system. The 293T cells in the culture medium were transferred into the central stream of the electroporation buffer by the DLD medium exchange module and then were transported to the OIE module for electroporation. The cells then flowed into the OIE zone, where the applied electric field induces a sufficient transmembrane potential across the cell for electroporation. The processing of 250 µl of culture medium with suspended cells at a flow rate of 25 µl min⁻¹ took approximately 10 min. The fluorescence intensity of the expressed EGFP plasmid was measured using a flow cytometer (BD ACCURI C6, USA). The expressed percentage of green fluorescence signal increased with the increasing applied peak-to-peak voltage in the OIE module. The highest efficiency of 8.3% occurred at 40 Vpp. This efficiency is the highest transfection efficiency ever demonstrated among existing OIE methods[19]. Note that the light irradiance on the OIE zone was 1.5 W cm⁻² and the volumetric flow rates of both liquid streams were 25 µl min⁻¹. In addition to single DNA
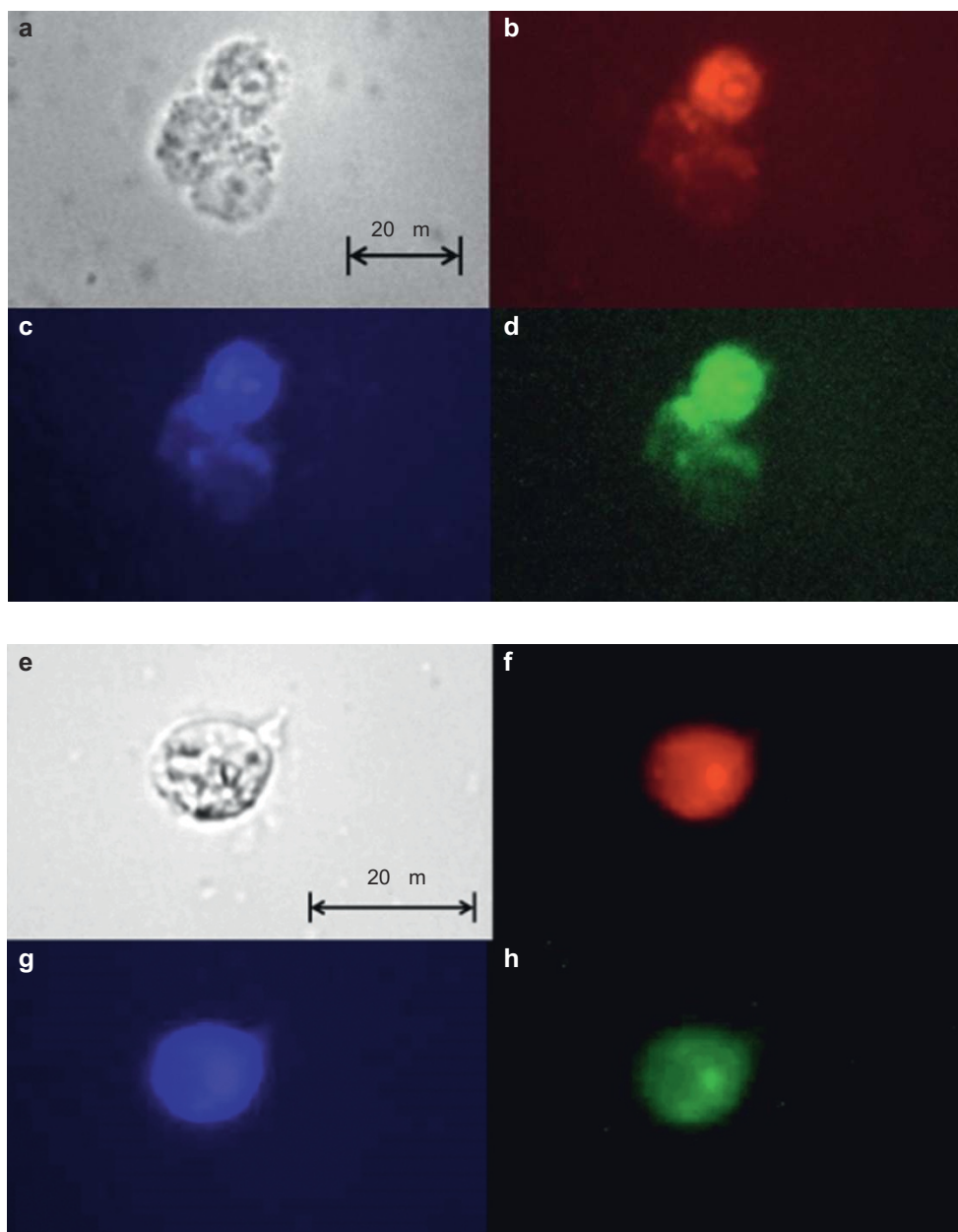
Figure 6 In the OIE module, HEK 293T cells, immersed in the electroporation buffer with plasmid DNA, flowed through the OIE zone (highlighted by the dashed line) and underwent electroporation. The inlet volumetric flow rates of the liquid streams were both 25 µl min^{-1}, and the electroporation duration for each cell was approximately 40 ms. The optical pattern was several times larger than the diameter of the cells to facilitate the electroporation of the cells to ensure full coverage of the OIE zone across the channel and to extend the duration for electroporation. A bright field image **(a)** and fluorescent images **(b–d)** of an HEK 293T cell 24 hours after the DLD-OIE system treatment. The fluorescent images **(f–h)** show that three distinct fluorescently labelled plasmids (DsRed, ECFP and EGFP) were successfully co-transfected into a single cell by using the OIE module integrated with the µPAR medium exchange module. The volumetric flow rates of the medium and the buffer solutions were both 90 µl min^{-1}. The light irradiance on the OIE zone was 1.5 W cm^{-2} and the applied voltage was 40 Vpp at a frequency of 20 kHz.

transfection, co-transfection of three plasmid DNAs into a single cell was also determined by the developed system, as shown in Figure 6a and 6d. The co-transfection into HEK 293T cells of pDsRED, pECFP and pEGFP-N1, which were red, blue and green fluorescently labelled plasmids, respectively, were successfully electroporated by using the DLD-OIE system (Figure 6b–d) and the µPAR-OIE system (Figure 6e–h), as verified by using an upright fluorescence microscope (BX43, Olympus Co., Japan) after

24 hours in culture. Note that the light irradiance on the OIE zone was 1.5 W cm^{-2}. The applied voltage was 40 Vpp at a frequency of 20 kHz. These images demonstrated that the novel microfluidic system successfully combined continuous medium exchange and optically electroporation modules to automatically perform the entire protocol for the transfection of exogenous molecules from re-suspended cells to electroporation. Note that all cells were viable after the transfection process was completed.

DISCUSSION

Cell debris was observed in the channel and between the microposts of the µPAR medium exchange module, as well as in the DLD medium exchange module. This debris can reduce the number of cells collected at the central outlet of the medium exchange module and compromise the medium exchange efficiency. The formation of the debris from the disruption of these cells could result from the high fluidic shear stresses experienced during the medium exchange process at high flow rates, where the cells are forced to change their direction in the fluid flow after sliding through the microposts of the µPAR structures. The average fluid velocity in this study (approximately 6 mm s^{-1} at a volume flow rate of 90 µl min^{-1}) was two to three times higher than the fluid velocity used in the previous study with biological cells (2.3 mm s^{-1}) where the observed railing failure rates (RFRs) were equivalent to 0%, i.e., no clogging of cells was observed[31]. However, reducing the fluid velocity would compromise the throughput of the medium exchange system and the overall transfection efficiency of the integrated microfluidic system. Therefore, a more thorough study of the relationship between shear-induced cell lysis and the fluid velocity in the medium exchange modules is required in the future. Another factor reducing the cell recovery rate was the cell clogging observed in the µPAR or DLD structures during experiments. In the µPAR medium exchange module, although the 10 µm gaps between microposts were smaller than the cell diameter (13 µm on average for HEK 293T cells), a certain percentage of the cells were still able to squeeze through the gaps or were trapped between posts due to their deformability, hence affecting the module performance. It is believed that the percentage of micropost gaps clogged by cells was inversely related to the volume flow rate. As the cells gained more momentum in the direction of the fluid along the channel, they were less affected by the fluid flowing through the gaps between the microposts, thereby reducing the possibility of being squeezed through or trapped in the gaps. The DLD structure, when compared with the µPAR structure, is ideally a clog-free cell separation method because the gaps are larger than the diameter of the cell of interest. However, factors such as variations in cell sizes, clumps of cells adhering together due to poor cell handling before the experiment, and insufficient surface pretreatment and modification to reduce cell adhesion could still result in the clogging of cells, as observed in the medium exchange experiments. Importantly, the cells were always filtered past a cell mesh filter before being injected into the device to ensure that only single cells were allowed into the module. Otherwise, lumps of multiple cells would be trapped in the gaps, thus defeating the purpose of the DLD structure. In addition, a protein-blocking surface treatment was required to prevent the cells from adhering to the PDMS surface because any attached cells would alter the hydrodynamic paths, and therefore adversely affect the cell recovery rate of the medium exchange module.

In this study, we demonstrated a new microfluidic OIE system integrated with the continuous medium exchange module to address the sample pre-treatment problem. The integrated microfluidic system was composed of two separated modules: the continuous medium exchange module (to automatically transfer the re-suspended cells into the specific electroporation buffer) and the OIE module (for cell electroporation). Two microfluidic cell separation methods, DLD and µPAR, were used in the design of two continuous medium exchange modules. Experimental results suggest that the µPAR structure outperformed the DLD structure in terms of exchange efficiency. This developed microfluidic system is the first integrated microfluidic optical electroporation system capable of performing continuous medium exchange on one device. Compared with previous work using micro-filtering devices for medium exchange, the current work allows for continuous separation of cells and medium exchange, thus increasing the throughput of the developed device[20]. DNA transfection can be performed using microelectrodes. However, microelectrodes require tedious fabrication processes. Both microelectrodes and optically assisted dielectrophoresis on a microsystem could be used for DNA transfection[19]. These approaches require the tested cells to be transfected with extracellular nucleic acids in a "static" situation. Our results represent the first time that the tested cells could be automatically transferred to a suitable transfection buffer and that DNA transfection could be performed in a continuous "flow-through" format. The throughput of the developed system depended on the volumetric flow rate of the culture medium and the concentration of the cells. For example, the throughput of the integrated microfluidic system was 2.5×10^4 cells per minute for the medium with 10^6 cells ml^{-1} at a volume flow rate of 25 µl min^{-1}, assuming no cell loss in the system. The throughput of the system could be increased by adjusting the flow rate and the cell concentration. However, the higher volumetric flow rate would reduce the electroporation duration in the OIE module and may affect the overall electroporation efficiency. Furthermore, the developed device achieved the highest gene transfection efficiency of 8.3% for EGFP, among all current OIE methods[14]. Moreover, co-transfection of multiple fluorescently labelled plasmids (EGFP, DsRed and ECFP) was confirmed. These results indicate that the developed device has great potential for use in various electroporation-related biological applications, such as creating induced pluripotent stem cells (iPSCs) and for gene therapy.

COMPETING INTERESTS

The authors declare no conflict of interest.

REFERENCES

1 Hou HW, Bhagat AAS, Lee WC *et al*. Microfluidic devices for blood fractionation. *Micromachines* 2011; **2**: 319–343.

2 Lenshof A, Laurell T. Continuous separation of cells and particles in microfluidic system. *Chemical Society Reviews* 2010; **39**: 1203–1217.

3 Bhagat AAS, Bow H, Hou HW *et al*. Microfluidics for cell separation. *Medical & Biological Engineering & Computing* 2010; **48**: 999–1014.

4 Pamme N. Continuous flow separations in microfluidic devices. *Lab on a Chip* 2007; **7**: 1644–1659.

5 Xuan X, Zhu J, Church C. Particle focusing in microfluidic devices. *Microfluid and nanofluid* 2010; **9**: 1–16.

6 Movahed S, Li D. Microfluidics cell electroporation. *Microfluid and nanofluid* 2011; **10**: 703–734.

7 Kim J, Hwang I, Britan D *et al*. Microfluidic approaches for gene delivery and gene therapy. *Lab on a Chip* 2011; **11**: 3941–3948.

8 Wang M, Orwar O, Olofsson J *et al*. Single-cell electroporation. *Analytical and Bioanalytical Chemistry* 2010; **397**: 3235–3248.

9 Potter H, Heller R. Transfection by electroporation. *Current Protocols in Neuroscience* 2011; Appendix 1: 1E.

10 Jordan ET, Collins M, Terefe J *et al*. Optimizing electroporation conditions in primary and other difficult-to-transfect cells. *Journal of Biomolecular Techniques* 2008; **19**: 328–334.

11 Pucihar G, Kotnik T, Kanduser M *et al*. The influence of medium conductivity on electropermeabilization and survival of cells in vitro. *Bioelectrochemistry* 2001; **54**: 107–115.

12 Lee WG, Demirci U, Khademhosseini A. Microscale electroporation: Challenges and perspectives for clinical applications. *Integrative Biology* 2009; **1**: 242–251.

13 Fei Z, Wang S, Xie Y *et al*. Gene transfection of mammalian cells using membrane sandwich electroporation. *Analytical Chemistry* 2007; **79**: 5719–5722.

14 Valero A, Post JN, van Nieuwkasteele JW *et al*. Gene transfer and protein dynamics in stem cells using single cell electroporation in a microfluidic device. *Lab on a Chip* 2008; **8**: 62–67.

15 Valley JK, Neale S, Hsu HY *et al*. Parallel single-cell light-induced electroporation and dielectrophoretic manipulation. *Lab on a Chip* 2009; **9**: 1714–1720.

16 Wang HY, Lu C. Electroporation of mammalian cells in a microfluidic channel with geometric variation. *Analytical Chemistry* 2006; **78**: 5158–5164.

17 Zhan Y, Wang J, Bao N *et al*. Electroporation of cells in microfluidic droplets. *Analytical Chemistry* 2009; **81**: 2027–2031.

18 Lin YH, Lee GB. An optically induced cell lysis device using dielectrophoresis. *Applied Physics Letters* 2009; **94**: 033901.

19 Wang CH, Lee YH, Kuo HT *et al*. Dielectrophoretically-assisted electroporation using light-activated virtual microelectrodes for multiple DNA transfection. *Lab on a Chip* 2014; **14**: 592–601.

20 Lee GB, Wu HC, Yang PF *et al*. Optically induced dielectropheresis sorting with automated medium exchange in an integrated optofluidic device resulting in higher cell viability. *Lab on a Chip* 2014; **14**: 2837–2843.

21 Beech JP, Holm SH, Adolfsson K *et al*. Sorting cells by size, shape and deformability. *Lab on a Chip* 2012; **12**: 1048–1051.

22 Huang LR, Cox EC, Austin RH *et al*. Continuous particle separation through deterministic lateral displacement. *Science* 2004; **304**: 987–990.

23 Holm SH, Beech JP, Barrett MP *et al*. Separation of parasites from human blood using deterministic lateral displacement. *Lab on a Chip* 2011; **11**: 1326–1332.

24 Inglis DW, Davis JA, Austin RH *et al*. Critical particle size for fractionation by deterministic lateral displacement. *Lab on a Chip* 2006; **6**: 655–658.

25 Davis JA, Inglis DW, Morton KJ *et al*. Deterministic hydrodynamics: Taking blood apart. *Proceedings of the National Academy of Sciences of the United States of America PNAS, Proceedings of the National Academy of Sciences* 2006; **103**: 14779–14784.

26 Morton KJ, Loutherback K, Inglis DW *et al*. Hydrodynamic metamaterials: Microfabricated arrays to steer, refract, and focus streams of biomaterials. *Proceedings of the National Academy of Sciences of the United States of America PNAS, Proceedings of the National Academy of Sciences* 2008; **105**: 7434–7438.

27 Green JV, Radisic M, Murthy SK. Deterministic lateral displacement as a means to enrich large cells for tissue engineering. *Analytical Chemistry* 2009; **81**: 9178–9182.

28 David WI, Megan L, Robert EN. Scaling deterministic lateral displacement arrays for high throughput and dilution-free enrichment of leukocytes. *Journal of Micromechanics and Microengineering* 2011; **21**: 054024.

29 Liu Z, Huang F, Du J *et al*. Rapid isolation of cancer cells using microfluidic deterministic lateral displacement structure. *Biomicrofluidics* 2013; **7**: 011801.

30 Karabacak NM, Spuhler PS, Fachin F *et al*. Microfluidic, marker-free isolation of circulating tumor cells from blood samples. *Nature Protocols* 2014; **9**: 694–710.

31 Sochol RD, Li S, Lee LP *et al*. Continuous flow multi-stage microfluidic reactors via hydrodynamic microparticle railing. *Lab on a Chip* 2012; **12**: 4168–4177.

32 Sochol RD, Corbett D, Hesse S *et al*. Dual-mode hydrodynamic railing and arraying of microparticles for multi-stage signal detection in continuous flow biochemical microprocessors. *Lab on a Chip* 2014; **14**: 1405–1409.

33 Chang CJ, Lu MY, Lee GB. A continuous optically-induced cell electroporation device with on-chip medium exchange mechanisms. IEEE 27th International Conference on Micro Electro Mechanical Systems (IEEE MEMS); 26–30 Jan 2014; San Francisco, CA, USA; **2014**: 234–237.

34 Le Gac S, van den Berg A. Single cell electroporation using microfluidic devices. *Methods in Molecular Biology* 2012; **853**: 65–82.